Determination of sea surface wind speed using the polarimetric and multidirectional properties of satellite measurements in visible bands

Tristan Harmel[1] and Malik Chami[1,2]

Received 8 August 2012; revised 11 September 2012; accepted 12 September 2012; published 12 October 2012.

[1] The reflection of the direct sunlight onto the rough sea surface (sun glint) generates a strong signal which is informative on wind speed. An original method is described to determine the wind speed values and their associated uncertainty over the ocean using multidirectional and polarimetric data measured by a passive satellite sensor in the visible/near infrared bands, namely PARASOL sensor. The method is able to derive wind speed values for almost 80% of a cloud-free scene. Comparisons with buoys and with the operational wind product of the AMSR-E sensor (NASA) show a satisfactory agreement (coefficient of correlation $r > 0.84$). This study demonstrates that passive satellite sensors that are able to measure the polarization and multidirectionality features of the radiation at solar wavelengths can be relevant alternative approaches to quantify the wind speed at a spatial resolution at least four times higher than that currently obtained using passive or active microwave sensors. **Citation:** Harmel, T., and M. Chami (2012), Determination of sea surface wind speed using the polarimetric and multidirectional properties of satellite measurements in visible bands, *Geophys. Res. Lett.*, *39*, L19611, doi:10.1029/2012GL053508.

1. Introduction

[2] Knowledge of surface winds is critically important for budgeting energy transport, oceanic primary productivity, studies of ocean acidification [*Dickey and Falkowski*, 2002; *Ohlmann and Siegel*, 2000]. Active and passive satellite remote sensing sensors that measure in the microwave spectral domain are commonly used to derive the wind speed values from space over the oceans with a spatial resolution varying between 25 km to 50 km and a typical accuracy of 1 m s^{-1} [*Bourassa et al.*, 2010].

[3] Passive remote sensing sensors working in the visible/near-infrared spectral range are generally not used for the purpose of wind speed determination because most of them do not provide sufficient physical information that is directly related to wind characteristics. The PARASOL ("Polarization and Anisotropy of Reflectances for Atmospheric Sciences Coupled with Observations from a Lidar") satellite sensor is currently the only one that is able to measure the multidirectional radiance and polarization state of light from space. Therefore, it provides substantial supplementary information relatively to monodirectional unpolarized visible/near-infrared radiometers. *Bréon and Henriot* [2006] showed using the previous generation of PARASOL sensor, namely the POLDER ("POLarization and Directionality of the Earth's Reflectances") sensor, that the unpolarized radiance measured at observation geometries for which the radiance is the most highly sensitive to sun glint may be exploited to accurately characterize the sea surface wind when wind speed values are lower than 14 m s^{-1}. However, the wind estimation based on their approach was limited (i) to the use of a restricted number of viewing directions given a pixel, (ii) to the use of the scalar radiance only (i.e., unpolarized light) and (iii) to a reduced spatial resolution of 50 km. In the current study, the capabilities of using all the viewing directions that are available for a given pixel together with the polarized information measured by PARASOL are investigated to derive sea surface wind speed over the full swath of the satellite at an interestingly high spatial resolution (typically 6 km). An inverse method which exploits the sun glint radiation measured from space at short wavelengths (visible/near infra-red bands) rather than at microwave bands is proposed to quantify the wind speed values.

2. PARASOL Sensor

[4] The PARASOL satellite sensor is orbiting among the five sun-synchronous satellites, forming the so-called A-Train. The originality of PARASOL sensor mostly relies on its capability to measure the polarization state of light (namely the Stokes parameters I, Q and U) for various wavelengths and for a high number of directions (up to 16 directions). The PARASOL spatial resolution is 6 km per 7 km at nadir viewing direction. The total acquisition time for a full multidirectional sequence is performed within 4-minute time period which is sufficiently short to assume that the geophysical parameters (such as wind properties) do not vary significantly during the acquisition period. The PARASOL measurements are performed in visible/near infrared bands, typically from 443 nm to 1020 nm.

3. Modelling of the Top of Atmosphere Signal

[5] The Stokes vector $\mathbf{S} = [I, Q, U, V]^T$ describes the electromagnetic radiation, including its polarization state, in terms of directly measurable quantities. At the top of the atmosphere, the signal received by a satellite sensor over the ocean for a given viewing geometry can be schematically decomposed as follows:

$$\mathbf{S_{TOA}} = T_g\left(\mathbf{S_{atm}} + T\mathbf{S_g} + t_d\mathbf{S_{wc}} + t_d\mathbf{S_w^+}\right) \quad (1)$$

[1]Laboratoire Océanographie de Villefranche, Université Pierre et Marie Curie, CNRS, Villefranche-sur-Mer, France.
[2]Institut Universitaire de France, Paris, France.

Corresponding author: T. Harmel, Laboratoire Océanographie de Villefranche, Université Pierre et Marie Curie, CNRS, BP 08, F-06230 Villefranche-sur-Mer CEDEX, France. (harmel@obs-vlfr.fr)

0094-8276/12/2012GL053508

where T_g is the transmittance due to the absorption of the atmospheric gases, T is the atmospheric direct transmittance, and t_d is the atmospheric diffuse transmittance. $\mathbf{S_{TOA}}$ is the Stokes vector at the top-of-atmosphere (TOA). $\mathbf{S_{atm}}$, $\mathbf{S_g}$, $\mathbf{S_{wc}}$ and $\mathbf{S_w^+}$ hold for the atmospheric component of the Stokes vector, the sun glint component of the Stokes vector, the whitecap component and the water-leaving component of the Stokes vector, respectively.

[6] An atmospheric correction algorithm, the so-called POLAC algorithm, which fully exploits the multidirectional and polarization features of the PARASOL sensor, was recently developed [*Harmel and Chami*, 2011]. The POLAC algorithm uses an optimization scheme for retrieving aerosol parameters such as the aerosol optical thickness and the water-leaving radiance. The POLAC algorithm also permits (i) the estimation of the uncertainty on the retrieved aerosol optical thickness which may originate from environmental effects (e.g., whitecaps contribution), and (ii) the estimation of the unpolarized and polarized sun glint radiation. In the current study, the POLAC algorithm is used to retrieve the atmospheric contribution ($\mathbf{S_{atm}}$) and the underwater contribution $\mathbf{S_w^+}$ of the Stokes vector. Ultimately, the sum of sun glint and whitecaps signal at TOA ($\mathbf{S_{g+wc}} = T\mathbf{S_g} + t_d\mathbf{S_{wc}}$) can be derived from the PARASOL data without any *a priori* assumption on the sea surface conditions.

4. Inversion Methodology for Estimating the Wind Speed

[7] The proposed method for estimating the surface wind speed values relies on the comparison between the sun glint/whitecaps contribution $\mathbf{S_{g+wc}}$ retrieved by POLAC and their simulated values modeled based on a series of parameters that include wind speed values. In this section, the forward model that is used to simulate the sun glint/whitecap contributions and the inverse method are presented.

4.1. Modeling the Wind-Related Signal

[8] Based on measurements that covered a wind speed range varying from 0 m s^{-1} to 14 m s^{-1}, Cox and Munk showed that the ocean surface can be modeled using a distribution of small facets which are oriented following a near-Gaussian distribution, namely a Gram-Charlier series [*Cox and Munk*, 1954]. This distribution can be expressed as a function of the crosswind and upwind components of the wave slope z_c and z_u, respectively, which are related to wind direction:

$$p(z_c,z_u) = \frac{1}{2\pi\sigma_c\sigma_u}\exp\left(-\frac{\xi^2+\eta^2}{2}\right)\left[1-\frac{C_{21}}{2}(\xi^2-1)\eta - \frac{C_{03}}{6}(\eta^2-3)\eta+\frac{C_{40}}{24}(\xi^4-6\xi^2+3) + \frac{C_{22}}{4}(\xi^2-1)(\eta^2-1)+\frac{C_{04}}{24}(\eta^4-6\eta^2+3)\right] \quad (2)$$

Here, $\xi = z_c/\sigma_c$ and $\eta = z_u/\sigma_u$ where σ_c and σ_u are the crosswind and upwind root mean squares components to the total variance of the slope distribution. The *Cij* coefficients quantify the non-Gaussian nature of the distribution. *Bréon and Henriot* [2006] refined the parameterization of the *Cij* coefficients which was shown to be highly relevant to describe actual observations [*Zhang and Wang*, 2010]. The Stokes sun glint vector $\mathbf{S_g}$ is obtained using the distribution function expressed in equation (2).

[9] The fraction of the ocean surface that is covered by sea foam is defined as whitecap coverage (hereafter noted as f_f). The modeling of f_f as a function of the surface wind speed variable (noted *ws*, in m s^{-1}) is often used [*Anguelova and Webster*, 2006]. In the current study, the optimal power-law formula obtained by [*Monahan and O'Muircheartaigh*, 1980] is used (equation (3)):

$$f_f = 2.95\ 10^{-6}\ ws^{3.52} \quad (3)$$

The Stokes vector of the sun glint/whitecaps contributions to the TOA Stokes vector can finally be modeled as:

$$\mathbf{S_{g+wc}} = (1-f_f)T\mathbf{S_g} + f_f t_d \mathbf{S_{wc}} \quad (4)$$

The radiance term I_{wc} of the $\mathbf{S_{wc}}$ vector is calculated by considering the average foam reflectance assumed to be equal to 0.13 at 865 nm [*Frouin et al.*, 1996; *Kokhanovsky*, 2004]. The foam reflectance is assumed to be totally unpolarized (i.e., $Q_{wc} = 0$ and $U_w = 0$). The direct and diffuse atmospheric transmittances are computed based on the aerosols optical thicknesses that are retrieved by the POLAC algorithm.

4.2. Inverse Method

[10] Based on the estimation of the glint/whitecaps contributions to TOA signal using PARASOL data, hereafter noted as $\mathbf{S^*_{g+wc}}$, and using the forward model of $\mathbf{S_{g+wc}}$, we can construct the following cost function $\Phi(\mathbf{x})$:

$$\Phi(\mathbf{x}) = \|\mathbf{S^*_{g+wc}} - \mathbf{S_{g+wc}}(\mathbf{x})\|^2 \quad (5)$$

The minimization of such a cost function permits to retrieve the parameter $\mathbf{x}$ which corresponds to the wind speed here. Note that the forward model suffers from ambiguities in the wind direction (i.e., given a wind speed value, fairly similar solutions could be obtained for different values of the wind azimuth) [*Bréon and Henriot*, 2006]. The complex problem of retrieving the wind azimuth from optical measurements is therefore not investigated in this study which focuses on retrieval of wind speed and its associated uncertainty. Due to the non-linearity of the inverse problem, iterative procedures that include the use of derivatives (Jacobians) to determine the local topography of the cost function need to be used. The Levenberg-Marquardt damped least-squares method is an extremely powerful tool for finding the iterative solution of nonlinear problems [*Pujol*, 2007]. Such a method was used here to minimize the cost function. The Levenberg-Marquardt method also enables to derive the uncertainty that is associated with the retrieved parameter. The uncertainty of the parameter $\mathbf{x}$ denoted as σ, expresses the sensitivity of the cost function to a variation of $\mathbf{x}$ lower than σ around the solution $\mathbf{x}$. It could be mathematically written as:

$$\begin{aligned} &|x - x'| \le \sigma \\ &\Phi(\mathbf{x}) \le (1+\varepsilon)\phi(\mathbf{x}') \end{aligned} \quad (6)$$

where $\mathbf{x}'$ is a point in the neighborhood of $\mathbf{x}$ and ε is a fixed coefficient describing the upper limit of the sensitivity of the cost function for an acceptable solution. In this study, ε was set to 5%.

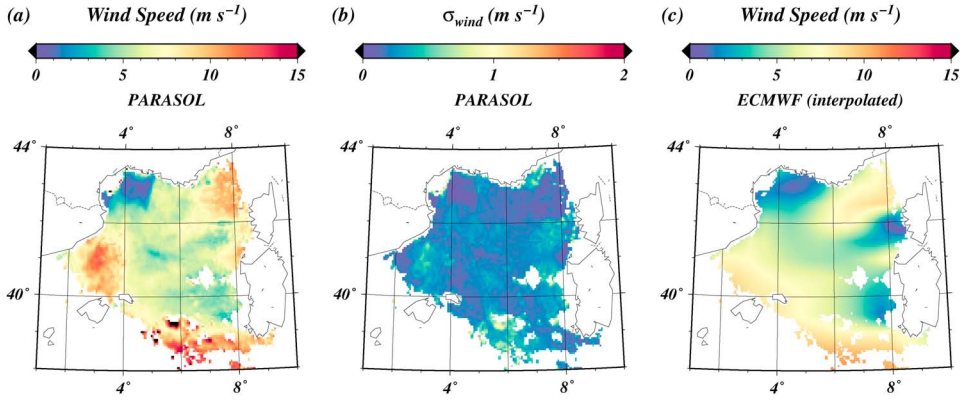

Figure 1. (a) Wind speed values and (b) their associated uncertainties, σ_{wind} (in m s^{-1}), retrieved from the PARASOL image acquired on May 5, 2006 over the north-west part of the Mediterranean Sea, (c) wind speed values as retrieved from the ECMWF database (for the same spatial resolution as PARASOL).

[11] Inverse methods are generally sensitive to the initial values used to start the iteration process. The strategy adopted here is as follows. First, the inverse method is independently applied starting from three initial values of wind speed: 1, 6 and 12 m s^{-1}. If the three obtained solutions are different from the respective initial values, the mean value of the solutions is used as first guess to start the final iteration of the procedure. If the solutions do not depart from the initial values, this means that the multidirectional and polarized acquisitions of the studied pixel are not sufficiently informative on wind speed. Then, in this latter case, the PARASOL pixel is flagged out.

5. Results and Discussion

[12] The inverse method is now applied to PARASOL level 1 images. Figure 1 shows the wind speed values (Figure 1a) and their associated uncertainties (Figure 1b) retrieved from a PARASOL image acquired on May 5th, 2006 over the north-west Mediterranean basin. High wind speed values (~12 m s^{-1}) are observed in the western and southern parts of the image while low wind speed values (~5 m s^{-1}) are retrieved in the center of the image. The zones where high wind speed values are retrieved generally show higher uncertainties (i.e., ~0.7 m s^{-1}). These higher uncertainties are likely due to the presence of whitecaps. A zone of very weak wind speed values (ws < 2 m s^{-1}) is noticeable in the northern part of the image (~43°N) between 4°E and 5°E. Perhaps, the fact that such oceanic area is especially surrounded by the continent (Gulf of Lion) might explain the weak wind speed values. The uncertainties associated to the weak wind speed area are generally smaller than 0.3 m s^{-1} (Figure 1b). Thus, the sun glint multidirectional and polarized radiation is sufficiently sensitive to the wind speed parameter to allow to the method to identify low wind speed area with a satisfactory performance.

[13] Figure 1 also shows the wind speed values as modeled by the ECMWF model for the full spatial resolution of PARASOL (Figure 1c). The ECMWF model corroborates the real occurrence of the low wind speed area in the Gulf of Lion. The general trend of variation of the wind speed over the entire image is roughly consistent between PARASOL and ECMWF. However, a careful analysis shows that PARASOL data allow distinguishing the fine variation of the wind speed throughout the entire image. As an example, the discontinuity of the wind speed values observed by PARASOL at 43°N when moving eastward from 4.5°E to 5.5°E is not well reproduced by the ECMWF model. More interestingly, the strong wind speed gradient observed by PARASOL at 41°N between 3°E and 5°E (decrease of wind speed from West to East with a local minimum at 5°E) is not so pronounced in the ECMWF image. Therefore, knowledge of wind speeds at a spatial resolution as fine as PARASOL full resolution may have some important implication for modelling purposes. Typically, the assimilation of high resolution wind speed data into ECMWF model should improve the predictions related to the weather forecast. A higher spatial resolution of wind speed data could also improve the representation of dynamic structure like eddies or specific upwelling cells in coastal regions where the dynamic processes are complex [*Schaeffer et al.*, 2011]. Note, however, that the limitation of space borne wind speed product is that overestimation or underestimation of wind speed could happen locally due to the fact that it takes some time for the sea surface to react to wind variations.

[14] The wind speed values retrieved with PARASOL were compared with concurrent wind speed data derived by the passive microwave satellite sensor AMSR-E (NASA) [*Wentz and Meissner*, 2000]. The AMSR-E sensor is part of the A-train, thus permitting virtually coincident observations with the PARASOL sensor. To perform relevant comparisons with AMSR-E products, which were rigorously validated using in situ measurements, the PARASOL wind speed data were re-projected into the same 0.25° × 0.25° grid (i.e., spatial resolution of 25 km) as the AMSR-E data. Figure 2 shows that the wind patterns are fairly consistent between both sensors. In particular, the local minimum of wind speed values observed by PARASOL at 41°N and 5°E is well reproduced with AMSR-E data. The PARASOL wind products were quantitatively compared over the same area of Figure 2 with the wind speed measured by two buoys (Météo-France organization; [43.4°N, 7.8°E] and [42.1°N, 4.7°E]) for one entire year, namely 2006 (146 match-ups). The comparisons (Figure 3a) show a coefficient of correlation greater than 0.96. The value of the slope is 0.96 and the root-mean-square error is satisfactory (1.1 m s^{-1}). Therefore, the comparisons between the PARASOL wind speed product and in situ measurements from buoys confirm that

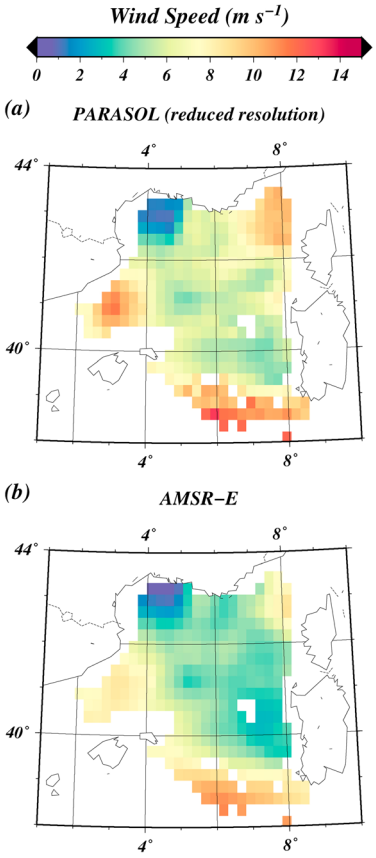

Figure 2. Wind speed values as retrieved for the same scene as Figure 1 from (a) PARASOL (after degradation of the spatial resolution from 6 km to 25 km to match to the AMSR-E resolution), (b) AMSR-E data.

the PARASOL space based measurements do not exhibit any systematic errors.

[15] The comparison is now generalized at global scale to get more quantitative results. PARASOL data acquired over three successive days, which correspond to the total revisit time of this satellite mission, were used. Figure 3b shows that a strong correlation coefficient (r = 0.84) is obtained between both sensors. The slope of the regression line points out an agreement within 1%. Note that the majority of the wind speed values encountered over the entire globe are within the range from 4 to 7 m s^{-1} (see gray color scale). The statistical parameters related to the comparison are reported in Table 1. The number of pixels used for wind speed retrieval represents almost 80% of the cloud-free measurements. Such a high ratio means that the inverse method could be used for performing a global scale analysis of the variation of wind speed and of its subsequent oceanographic/atmospheric applications. Table 1 also shows that the root- mean-square error (RMSE) between PARASOL and AMSR-E data is about 1.6 m s^{-1}. Such a RMSE value is in a good agreement with previous studies [*Bréon and Henriot*, 2006; *Freilich and Dunbar*, 1999].

6. Conclusion

[16] A methodology was investigated to accurately derive surface sea wind speed values from original multidirectional and polarimetric satellite measurements in the visible spectral domain. The approach relies on the fact that the sun glint pattern is directly dependent on wind speed. The strength of the method is to quantify the wind speed for a spatial resolution (i.e., 6 km × 7 km) which is much higher (by a factor of 4 to 8) than that which is typically obtained by usual satellite microwave sensors. Another originality is to provide estimates of the uncertainty in the retrieved wind speed, which is highly requested by data assimilation modelers or end-users. In this study, the retrieved uncertainty estimates of wind speed generally showed values smaller than 1 m s^{-1} which is satisfactory for most applications using wind data. Our statistical analysis highlighted that around ∼80% of the cloud-free pixels can be potentially used for wind speed determination. Such a wide spatial coverage indicates that the wind speed product could be combined with coincident aerosols and ocean color products. Thus, the wind speed product derived from satellite sensors measuring at short wavelengths should allow further investigations in various

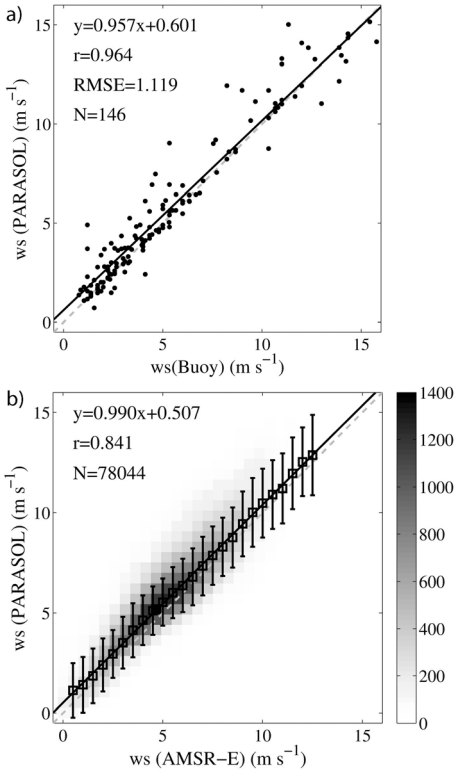

Figure 3. (a) Comparison of the wind speed values *ws* as retrieved from the PARASOL data with meteorological buoys data acquired over the year 2006 in the Mediterranean Sea. (b) Comparison of the wind speed values over the entire globe derived from PARASOL (y-axis) and AMSR-E (x-axis) measurements after re-projection of PARASOL data into the 0.25° × 0.25° AMSR-E grid. The comparison in Figure 3b is performed over three successive days (from May 5 to 7 2006) of global acquisitions over the ocean. The grey color scale is proportional to the density of points in bin of 0.5 m s^{-1}. The symbols and error bars indicate the median and standard deviation of PARASOL retrieved product. Equation of the regression line (black line) is given in the left upper corner; r is the correlation coefficient. N is the total number of match-ups used for the comparison.

Table 1. Statistics of PARASOL Images and Statistical Parameters Related to the Comparison Between the AMSR-E and PARASOL Retrieved Wind Speed Values Shown in Figure 3b

PARASOL Statistics (Full Spatial Resolution Data)	Value
Total number of pixels over ocean	$5.3\ 10^6$
Number of cloud-free pixels	$2.1\ 10^6$
Number of pixels used for wind retrieval	$1.7\ 10^6$
Statistical Parameters Related to the Comparison Between PARASOL and AMSR-E Sensors (Figure 3)	**Value**
Number of pixels used for wind retrieval (spatial resolution of AMSR-E data)	78044
Correlation coefficient	0.84
RMSE ($m\ s^{-1}$)	1.57

multidisciplinary topics such as studies dedicated to aerosol transport and marine primary productivity. The implications for determining the wind speed at a high spatial resolution are important as well for modeling and data assimilation purposes. The applications could concern the weather forecast predictions or the oceanic dynamic. The current study will be helpful as well to prepare the forthcoming satellite missions dedicated to the measurements of the multidirectional and polarimetric properties of the radiation such as the "Preparatory Aerosols, Clouds and Ecosystems (PACE)" mission (NASA) or the "Multi-directional, Multi-polarization and Multispectral (3MI)" mission (European Space Agency, ESA) which are both scheduled for launch around 2018.

[17] **Acknowledgments.** This research was supported by the French program Programme National de Télédétection Spatiale (PNTS). The authors would like to thank the organization ICARE (Laboratoire d'Optique Atmosphérique and Centre National d'Etudes Spatiales-CNES) for providing the PARASOL geophysical products. We also would like to thank the AMSR-E Science Team (NASA) and the ECMWF organization for providing the wind speed data. We are grateful to V. Taillandier for helpful discussions. The authors wish to thank the reviewers.

[18] The Editor thanks two anonymous reviewers for assisting in the evaluation of this paper.

References

Anguelova, M. D., and F. Webster (2006), Whitecap coverage from satellite measurements: A first step toward modeling the variability of oceanic whitecaps, *J. Geophys. Res.*, *111*, C03017, doi:10.1029/2005JC003158.

Bourassa, M., et al. (2010), Remotely sensed winds and wind stresses for marine forecasting and ocean modeling, in *Proceedings of the "OceanObs'09: Sustained Ocean Observations and Information for Society" Conference, Vol. 2*, edited by J. Hall et al., *Eur. Space Agency Spec. Publ.*, *WPP-306*, doi:10.5270/OceanObs09.cwp.08.

Bréon, F. M., and N. Henriot (2006), Spaceborne observations of ocean glint reflectance and modeling of wave slope distributions, *J. Geophys. Res.*, *111*, C06005, doi:10.1029/2005JC003343.

Cox, C., and W. Munk (1954), Statistics Of The Sea Surface Derived From Sun Glitter, *J. Mar. Res.*, *13*, 198–227.

Dickey, T., and P. Falkowski (2002), Solar energy and its biological-physical interactions in the sea, in *The Sea*, vol. 12, *Biological-Physical Interactions in the Sea*, edited by A. Robinson, J. J. McCarthy, and B. J. Rothschild, pp. 401–440, Harvard Univ. Press, Cambridge, Mass.

Freilich, M. H., and R. S. Dunbar (1999), The accuracy of the NSCAT 1 vector winds: Comparisons with National Data Buoy Center buoys, *J. Geophys. Res.*, *104*, 11,231–11,246, doi:10.1029/1998JC900091.

Frouin, R., M. Schwindling, and P.-Y. Deschamps (1996), Spectral reflectance of sea foam in the visible and near-infrared: In situ measurements and remote sensing implications, *J. Geophys. Res.*, *101*, 14,361–14,371, doi:10.1029/96JC00629.

Harmel, T., and M. Chami (2011), Influence of polarimetric satellite data measured in the visible region on aerosol detection and on the performance of atmospheric correction procedure over open ocean waters, *Opt. Express*, *19*, 20,960–20,983, doi:10.1364/OE.19.020960.

Kokhanovsky, A. A. (2004), Spectral reflectance of whitecaps, *J. Geophys. Res.*, *109*, C05021, doi:10.1029/2003JC002177.

Monahan, E. C., and I. O'Muircheartaigh (1980), Optimal power-law description of oceanic whitecap coverage dependence on wind speed, *J. Phys. Oceanogr.*, *10*, 2094–2099, doi:10.1175/1520-0485(1980)010<2094:OPLDOO>2.0.CO;2.

Ohlmann, J. C., and D. A. Siegel (2000), Ocean radiant heating. Part II: Parameterizing solar radiation transmission through the upper ocean, *J. Phys. Oceanogr.*, *30*, 1849–1865, doi:10.1175/1520-0485(2000)030<1849:ORHPIP>2.0.CO;2.

Pujol, J. (2007), The solution of nonlinear inverse problems and the Levenberg-Marquardt method, *Geophysics*, *72*, W1–W16, doi:10.1190/1.2732552.

Schaeffer, A., P. Garreau, A. Molcard, P. Fraunié, and Y. Seity (2011), Influence of high-resolution wind forcing on hydrodynamic modeling of the Gulf of Lions, *Ocean Dynamics*, *61*, 1823–1844, doi:10.1007/s10236-011-0442-3.

Wentz, F. J., and T. Meissner (2000), AMSR ocean algorithm, *Algorithm Theor. Basis Doc. 121599A-1*, Remote Sens. Syst., Santa Rosa, Calif.

Zhang, H., and M. Wang (2010), Evaluation of sun glint models using MODIS measurements, *J. Quant. Spectrosc. Radiat. Transfer*, *111*, 492–506, doi:10.1016/j.jqsrt.2009.10.001.